


## Article

# Service Life Prediction of Reinforced Concrete in a Sea-Crossing Railway Bridge in Jiaozhou Bay: A Case Study

Zhe Li <sup>1,2</sup> , Zuquan Jin <sup>1,2,\*</sup>, Tiejun Zhao <sup>1,2</sup>, Penggang Wang <sup>1,2</sup>, Lixiao Zhao <sup>1,2</sup>, Chuansheng Xiong <sup>1,2</sup> and Yue Kang <sup>1,2</sup>

<sup>1</sup> School of Civil Engineering, Qingdao University of Technology, Qingdao 266033, China

<sup>2</sup> Cooperative Innovation Center of Engineering Construction and Safety in Shandong Blue Economic Zone, Qingdao 266033, China

\* Correspondence: jinzuquan@126.com

Received: 24 July 2019; Accepted: 22 August 2019; Published: 1 September 2019



**Abstract:** Reinforced bar corrosion induced by chloride ingress is one of the most significant threats to the durability of concrete structures in marine environments. The concrete cover thickness, compressive strength, chloride diffusion coefficient, and surface defects of reinforced concrete in the Jiaozhou Bay sea-crossing railway bridge were measured. The temperature and relative humidity in the concrete and the loading applied onto the reinforced concrete were monitored. Based on the DuraCrete model, a revised model for the service life prediction of concrete structures was established, considering the effects of temperature and loading on the chloride diffusion coefficient. Further, the reliability indexes of the reinforced concrete box girder, pier, and platform, located in the marine and land sections, in relation to service lives lasting various numbers of years, were calculated. The measured and calculated results show that the mean cover thicknesses of concrete piers in the marine and land sections are 52 mm and 36 mm, respectively, and the corresponding standard deviations are 5.21 mm and 3.18 mm, respectively. The mean compressive strengths of concrete in the marine and land sections are 56 MPa and 46 MPa, respectively. The corresponding standard deviations are 2.45 MPa and 2.67 MPa, respectively. The reliability indexes of the reinforced concrete box girder and platform in the marine section, under the condition of a service life of 100 years, are 1.81 and 1.76, respectively. When the corrosion-resistant reinforced bar was used in the pier structure in the marine section, its reliability index increased to 2.01. Furthermore, the reliability index of the reinforced concrete damaged by salt fog in the land section was 1.71.

**Keywords:** reinforced concrete; sea-crossing railway bridge; service life prediction; reliability index

## 1. Introduction

With the development of modern society and technology, more and more huge reinforced concrete (RC) structures have been built in China [1–3], such as Hong Kong-Zhuhai-Macau (HZM) bridge (49.968 km long, in service), Hangzhou Bay bridge (36 km long, in service) and Jiaozhou Bay bridge (36.48 km long, in service). As reinforced concrete sea-crossing bridges service in marine environments, chloride ions penetrate the concrete cover and result in the corrosion of the reinforced bars, thereby causing serious damage to the bridge structures [4–8]. Many problems caused by the corrosion of reinforced bars have been reported all over the world. Further, corrosion-associated maintenance and repair of reinforced concrete (RC) structures have cost multiple billions of USD per annum [9]. In some developed countries, nearly 3.5% of their gross national product (GNP) has been applied in the repair cost [10]. In order to reduce the repair cost, the durability design of RC structures,

in particular, those exposed to marine environments, has been recognized as an effective means to ensure the service life of concrete structures, which has been a focus of researchers and engineers all over the world [11–13].

Service life prediction modeling has become one of the current major issues in the design of concrete structures. Using the third-moment method, Zhang [14] developed a time-dependent probability assessment for chloride-induced corrosion of RC structures. In order to provide corrective parameters for service life prediction, Li [15] investigated the time-dependent chloride penetration into concrete in marine environments. Considering the effect of the materials' heterogeneity when exposed to a marine tidal zone, Wang [16] developed a service life prediction model. Attari and McNally [17] explored a probabilistic assessment of the influence of the age factor on the service life prediction using concrete with limestone cement/ground granulated blast slag (GGBS) binders. Yu [18,19] developed a service life prediction model considering freeze–thaw fatigue, taking into account fly ash and slag. Hackl and Kohler [20] developed a reliability assessment which uses the coupled effect of corrosion initiation and progression to represent the deterioration of reinforced concrete structures. Considering the action of loading, chloride ions' transport path, and the binding capacity of concrete, a series of service life prediction models were developed by Sun [21]. Based on the experimental and theoretical studies on chloride transportation into concrete in marine environments, a service life prediction model was developed in DuraCrete, Life 365, and Chinese code for the durability design of concrete structures. However, Hostis [22] highlighted that most of the experimental studies on the corrosion of reinforced concrete structures are tested in the laboratory by means of accelerated measurement. Hence, the experimental data may not be representative compared to the "in situ" behavior. Samson [23] also emphasized that it is undesirable to predict the long-term service life of structures on the basis of laboratory sample measurements, which is a limitation to reliable predictions. Further, the measurement results obtained by Jin [24,25] showed that there were fluctuations in the durability parameters of lining concrete, such as concrete cover, concrete strength, and chloride diffusion coefficient, in the Jiaozhou Bay subsea tunnel, and the service life was also predicted. However, there is still limited research on the service life prediction of real marine projects, such as sea-crossing bridges, offshore platforms, and subsea tunnels.

The Jiaozhou Bay sea-crossing railway bridge is about 16.337 km long, and 2.006 km is in the marine area. It is the control bridge for the Qingdao–Lianyungang city railway network. At Qingdao, where the bridge is located, the relative humidity is 62–86%, which is the most suitable humidity range for carbonation. The chloride content in the seawater is about 16,000 mg/L, and the annual average sea fog days is about 58 days. Hence, the penetration of chloride ions into concrete is seriously threatening the durability of the bridge. In order to improve the concrete durability of the Jiaozhou Bay sea-crossing railway bridge, high-performance concrete and corrosion-resistant reinforced bars have been used in the pier structures, which are in the marine tidal and splash zones. The values of the key durability coefficients, such as the chloride diffusion coefficient of concrete, concrete cover thickness, and curing age of reinforced concrete, have been assigned based on the Chinese durability design code. However, the difference in the quality control of the concrete structure on site causes the durability index of the reinforced concrete to fluctuate. Therefore, the actual service life of the reinforced concrete may not meet the designed service life of the Jiaozhou Bay sea-crossing railway bridge.

The objectives of this study are to determine the actual durability coefficient of the concrete in the Jiaozhou Bay sea-crossing railway bridge, and to monitor the environmental temperature, relative humidity, and the loading applied onto the reinforced concrete. Based on the measured durability parameters of concrete, the actual service life of the reinforced concrete in the Jiaozhou Bay sea-crossing railway bridge, in different structures, is predicted according to the revised DuraCrete model.

## 2. Materials and Mix Proportion of Concrete

A Chinese standard 52.5 R(II) Portland cement was supplied by Shanshui cement corporation in China. Class F fly ash was used as a mineral admixture. River sand with a fineness modulus of 2.5 and

coarse aggregates of crushed stone with sizes of 5–10 mm, 10–20 mm, and 20–31.5 mm from Daxin Corporation were used. A new type of corrosion-resistant reinforced bar, Cr10Mo1 alloy, was used in the cross-sea section of the concrete bridge, as shown in Figure 1. The new type of reinforced bar is alloyed with about wt.10% Cr and wt.1% Mo, consisting of granular bainite with ferrite between the grains, and was developed by Southeast University [26]. Laboratory tests showed that the Cr10Mo1 reinforced bar has a critical chloride threshold level five times higher than that of carbon steel [27]. This is the first time that this new type of alloy has been used in a huge construction project in China, and the price is about 8000 RMB per ton (equal to 1140 USD per ton, approximately). The chemical compositions of the CR (corrosion-resistant reinforced bar) and LC (low-carbon steel) are shown in Table 1.

**Table 1.** Chemical compositions of corrosion-resistant (CR) and low-carbon (LC) steel.

Type	Chemical Composition (wt. %)								
	Fe	C	Si	Mn	P	S	V	Cr	Mo
CR	Bal.	0.01	0.49	1.49	0.01	0.01	0.06	10.36	1.16
LC	Bal.	0.22	0.53	1.44	0.02	0.02	0.04	/	/

According to the service environment, two types of high-performance concrete were used in the pier structures of the Jiaozhou Bay sea-crossing railway bridge. One type is C40 concrete with water/cement ratio ( $w/b$ ) = 0.33 and was used in the land section. The other type is C50 concrete with  $w/b$  = 0.3 and was used in the marine section. The mixture proportions for the two types of concrete are shown in Table 2. After curing the concretes in a standard room for 28 days, the compressive strengths of the two types of concrete were 47.5 MPa and 58.2 MPa, respectively.

**Table 2.** Mix proportions of concrete used in the land and marine sections ( $\text{kg}/\text{m}^3$ ).

Component	Cement	Fly Ash	Aggregate (mm)			Sand	Water	Super Plastizer	Air Entraining Agent
			5–10	10–20	20–31.5				
Land section	315	135	207	414	414	721	149	4	2.7
Marine section	336	144	208	416	416	709	144	5.28	2.88



**Figure 1.** Reinforced concrete pier of the Jiaozhou Bay sea-crossing railway bridge (marine section).

### 3. Durability Coefficients of Constructed Reinforced Concrete

#### 3.1. Concrete Cover Thickness and Compressive Strength

The service life of reinforced concrete was determined by concrete cover thickness and its properties, and the margins for the cover thicknesses suggested by DuraCrete were 20 mm, 14 mm, and 8 mm, which represent high, normal, and low repair cost, respectively. The concrete compressive

strength was measured by a rebound apparatus (manufactured by Runjie Corporation), and also the cover thickness of the pier structures was tested by a cover thickness meter (manufactured by Meiyu Corporation), as shown in Figure 2. The actual concrete cover of the reinforced concrete piers in Jiaozhou Bay sea-crossing railway bridge is shown in Figure 3. The measured concrete cover thickness of the piers in the marine and land sections followed a normal distribution. The mean cover thicknesses of the concrete piers in the marine and land sections were 52 mm and 36 mm, respectively. The corresponding standard deviations were 5.21 mm and 3.18 mm, respectively. The maximum difference between the measured and designed cover thicknesses of the concrete piers was less than 15 mm. Therefore, to ensure that the concrete is made more durable, it is very important to control the cover thickness in situ.

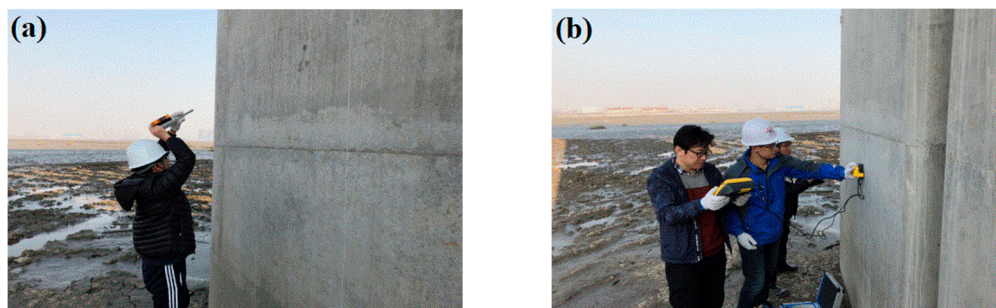


**Figure 2.** Rebound strength and cover thickness tests at piers. (a) Rebound strength; (b) Cover thickness.

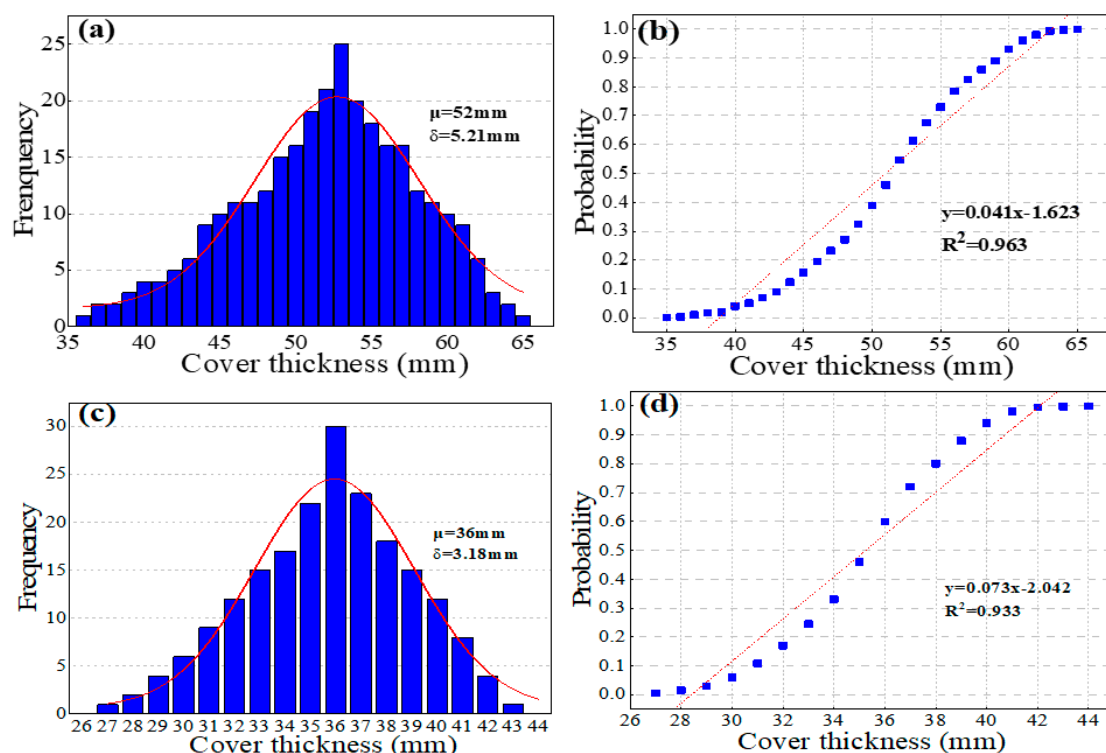


**Figure 3.** Concrete cover thickness of piers in the marine section and the land section. (a) Frequency (marine section); (b) Probability (marine section); (c) Frequency (land section); (d) Probability (land section).

After curing in situ, the compressive strength and rebound strength of the casting concrete specimens ( $100\text{ mm} \times 100\text{ mm} \times 100\text{ mm}$ ) used in the marine and land sections were measured by a compression-testing machine and rebound hammer, respectively. As shown in Figure 4, the linear relationships between the compressive strength and the average rebound strength of the concrete



specimens were obtained. In order to evaluate the actual compression strength of the large volume of pier concrete (exceeding 300 m<sup>3</sup>), the rebound strengths of the pier concrete in the marine and land sections were measured by a rebound hammer, and then the compressive strengths were calculated using the regressed linear relationships (Figure 4) based on the measured rebound strengths, which are shown in Figure 5. The compressive strengths of the concrete in the marine and land sections also follow a normal distribution. Further, the mean compressive strengths of concrete in the marine and land sections are 56 MPa and 46 MPa, respectively. The corresponding standard deviations are 2.45 MPa and 2.67 MPa, respectively. The designed compressive strengths of the concrete in the marine and land sections are 50 MPa and 40 MPa, respectively. Hence, the actual mean compressive strength of the concrete is higher than the designed strength. However, the minimum measured compressive strength is less than the designed strength, by about 7.2%.

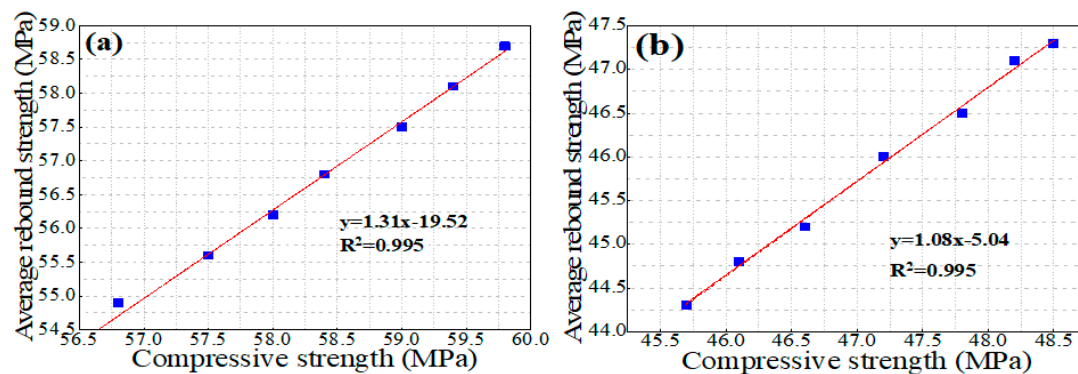


**Figure 4.** Linear relationships between compressive strength and average rebound strength for concrete in the marine and land sections. (a) Marine section; (b) Land section.

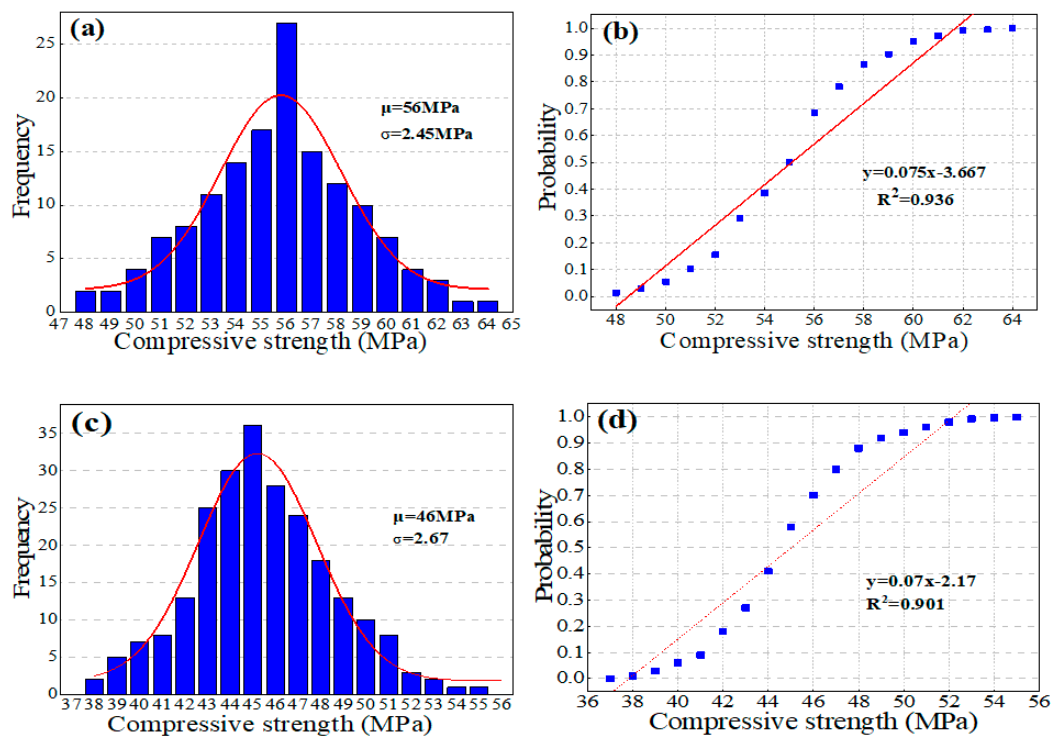


**Figure 5.** Compressive strength of piers in the marine section and the land section (a) Frequency (marine section); (b) Cover thickness probability (marine section); (c) Frequency (land section); (d) Cover thickness probability (land section).

### 3.2. Concrete Surface Defects

Concrete surface defects, such as air bubbles and exposed aggregates, shorten the chloride ions' migration depth. A digital camera was used to capture the surface morphology of the concrete pier in the marine section. The images show that there are a number of tiny holes and bubbles caused by inadequate vibration of concrete on the surface. Using Image Pro Plus software, the color uniformity, bubble number, and area on the surface of the reinforced concrete were calculated, as shown in Figure 6. Figure 6b shows that the standard deviation of the gray level of the eastern concrete pier surface is 22.05 pixels. This is an indication that the concrete surface is relative shiny. Further, the relationship between the bubble area and the number of bubbles can be expressed by a power function. Bubbles with small areas (i.e., 4–9 mm<sup>2</sup>) represent the largest percentage of the total bubble number. On the other hand, bubbles with large areas (i.e., 49–174 mm<sup>2</sup>) represent the largest percentage of the total bubble area. This is because the large-area bubbles can easily break up into many small-area bubbles during construction, and the small-area bubbles cannot be easily removed.

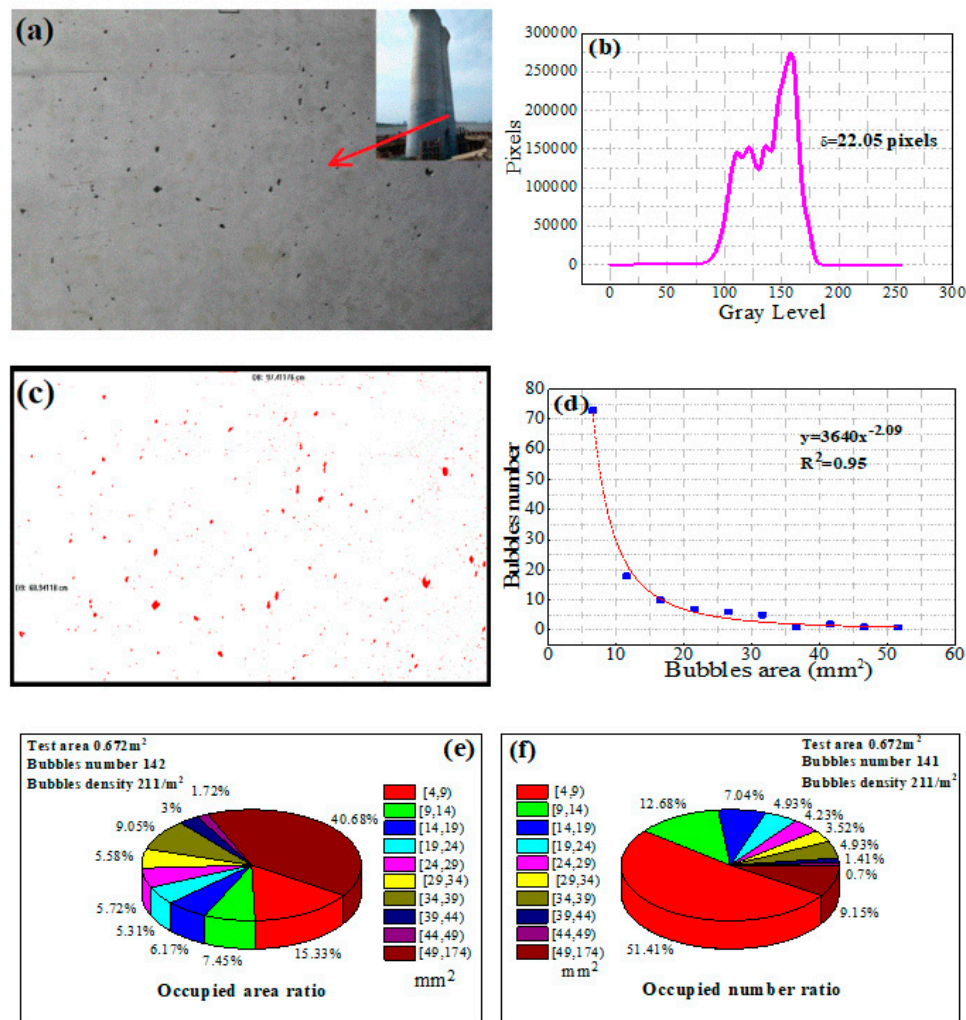


**Figure 6.** Concrete surface defects. (a) Concrete surface; (b) Gray level processing; (c) Bubble area calculation; (d) Relationship between bubble area and bubble number; (e) Percentage of bubbles area occupied; (f) Percentage of bubble number occupied.

### 3.3. Chloride Diffusion Coefficient

The rapid chloride migration (RCM) test was conducted to determine the apparent chloride diffusion coefficient of the concrete according to Chinese design code for marine concrete (GB/T

50476-2008) [28]. For the concrete used in the marine and land sections, after curing in situ for 28 days, the mean chloride diffusion coefficients were  $2.32 \times 10^{-12} \text{ m}^2/\text{s}$  and  $4.38 \times 10^{-12} \text{ m}^2/\text{s}$ , respectively. Zhao [29] reported that the relationship between the chloride diffusion coefficient and the compressive strength can be expressed by the exponential function. Figure 5 shows that the compressive strengths of concrete follow a normal distribution. Therefore, the mean chloride diffusion coefficients of concrete in the marine section and the land section are  $2.32 \times 10^{-12} \text{ m}^2/\text{s}$  and  $4.38 \times 10^{-12} \text{ m}^2/\text{s}$ , and their corresponding standard deviations are  $0.10 \text{ m}^2/\text{s}$  and  $0.23 \text{ m}^2/\text{s}$ , respectively.

For the reinforced concrete structure subjected to loading, the loading affects the chloride ions' penetration, and sulfate and frost damage to the concrete. Based on the assumption of uniaxial compression load, the influence of load level (the ratio of uniaxial load to the prismatic compressive strength of the concrete specimen) on the chloride ion diffusion coefficient can be ignored due to the excellent compressive strength of high-performance concrete when the stress level does not exceed 0.3 [30]. However, if the stress level is higher than 0.3, the diffusion coefficient of chloride ions will be increased because of the formation of micro-cracks inside the concrete. Hence, if the sustained loading effect is not taken into account in the assessment of the durability of the structure, this will give an inaccurate prediction of the service life of the structure [31]. In order to evaluate the stress applied on the concrete, six reinforced stress gauges were installed inside the concrete. Figure 7 shows the arrangement of the reinforced stress gauges. Due to the self-calibration process, the strain of the reinforced concrete can be calculated using the following equation:

$$\sigma = K[\varepsilon_0 - \varepsilon_i - K_T(T - T_0)] \quad (1)$$

where  $\sigma$  is the strain of the reinforced concrete,  $K$  is the coefficient of the monitoring sensor,  $\varepsilon_0$  is the initial strain,  $\varepsilon_i$  is the final strain,  $K_T$  is the temperature coefficient,  $T$  is the final temperature, and  $T_0$  is the initial temperature.

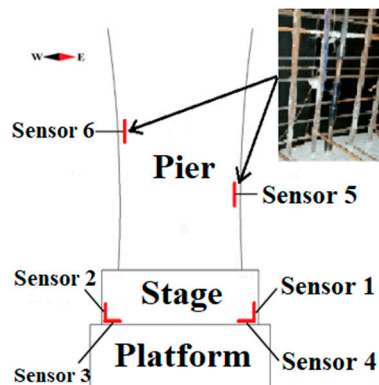


**Figure 7.** Schematic diagram of the arrangement of reinforced stress gauges in concrete piers.

Figure 8 shows that the stress applied onto the vertical bar decreases with time, and the stress applied onto the horizontal bar increases with time. Wan [32] developed a relationship between the axial load and the chloride ion diffusion coefficient of concrete, as shown in Table 3. Considering the effect of the loading and because of the measured stress applied onto the reinforced concrete, the enlargement coefficient  $k_s$  of 1.02 was selected.

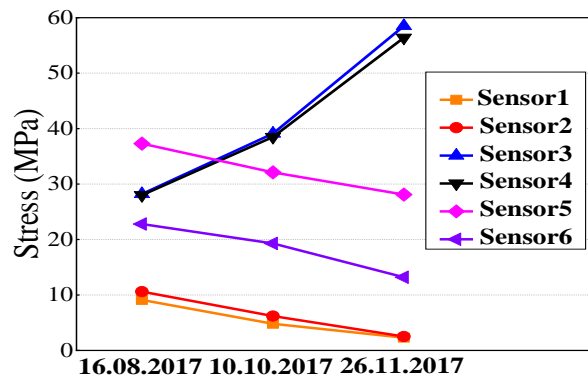


Figure 8. Variation of stress applied on reinforced bars with time.

Table 3. Relationship between axial load and the enlargement coefficient  $k_s$  of  $D_{RCM}$ .

	Loading Level	Enlargement Coefficient $k_s$ of $D_{RCM}$		Loading Level	Enlargement Coefficient $k_s$ of $D_{RCM}$
Concrete with fly ash	0	1	Concrete without fly ash	0	1
	0.2	0.90		0.2	0.98
	0.3	0.95		0.3	0.99
	0.5	1.02		0.5	1.04
	0.8	1.08		0.8	1.17

### 3.4. Temperature and Relative Humidity Evolution in Concrete

The temperature and relative humidity (RH) in concrete affects the chloride ions' transportation, and large changes in temperature and RH can even cause the concrete to crack. High temperature will increase the migration capacity of chloride ions in concrete, considering the time-varying performance of temperature response, and thus the transport of chloride ions in concrete will be affected by temperature. Moreover, the internal temperature of concrete is greatly influenced by the service environment [33]. Temperature and humidity sensors were pre-embedded inside the concrete at a depth of 25 mm from the concrete surface, and a wireless transportation apparatus was used to collect the monitoring data automatically, as shown in Figure 9.



Figure 9. Sensor and apparatus. (a) Temperature and humidity sensor; (b) Wireless transportation apparatus (with solar panel).

Because the relative humidity in the marine section is often higher than 80%, the relative humidity in concrete in tidal zones is always 100%. Figure 10 shows the variation of the temperature inside the concrete as compared to the atmospheric temperature. It can be seen that the temperature inside the concrete is significantly affected by the atmospheric temperature, especially near the concrete surface. The principle of continuous temperature variation meets the regularity of the Fourier transform formula; hence, the formula of the temperature response inside the concrete was fitted as Equation (2) and Equation (3). After appropriately fitting, Equation (2) can be rewritten as Equation (4).



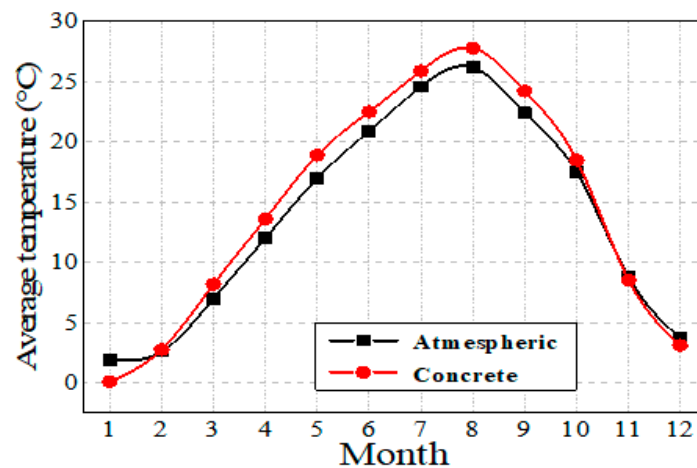


Figure 10. Comparison between atmospheric temperature and concrete temperature.

$$T(t) = T_a + \sum_{n=1}^{\infty} \left\{ A_n \cos \left[ \frac{2n\pi}{P} (t - t_0) \right] + B_n \sin \left[ \frac{2n\pi}{P} (t - t_0) \right] \right\} \quad (2)$$

$$\begin{cases} A_n = \frac{2}{P} \int_0^P T_a(t) \cos \left[ \frac{2n\pi}{P} (t - t_0) \right] dt \\ B_n = \frac{2}{P} \int_0^P T_a(t) \sin \left[ \frac{2n\pi}{P} (t - t_0) \right] dt \end{cases} \quad (3)$$

$$T = 16.64 + 14.38 \cos \left[ \frac{\pi}{6} (t - 7) \right] + 2.48 \cos \left[ \frac{\pi}{3} (t - 9.15) \right] \quad (4)$$

where  $T_a$  is the annual average temperature, °C;  $A_n$  and  $B_n$  are amplitude coefficients, respectively;  $t$  is time in months;  $t_0$  is the month that has the maximum average temperature; and  $P$  is 12 [34].

#### 4. Revised Service Life Prediction Model Suggested by DuraCrete

The performance evolution of a concrete structure with respect to reinforced corrosion and related events, from reinforced depassivation to construction collapse, is shown in Figure 11. During the first period, chloride ions penetrate into the concrete and induce the depassivation of the reinforced bar. This period is named the design service life of concrete in marine environments. Since there are fluctuations in the durability parameters of concrete, a reliability design is introduced into the durability design, and the design idea is shown in Figure 12. The probability of failure within the period  $[0, T]$  can be expressed by Equation (5), and the limit state function can be written as Equation (6). The service life prediction model of concrete in chloride environments, as suggested by DuraCrete, is shown as Equation (7).

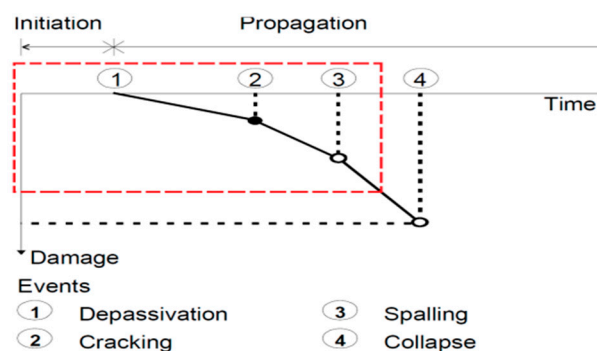
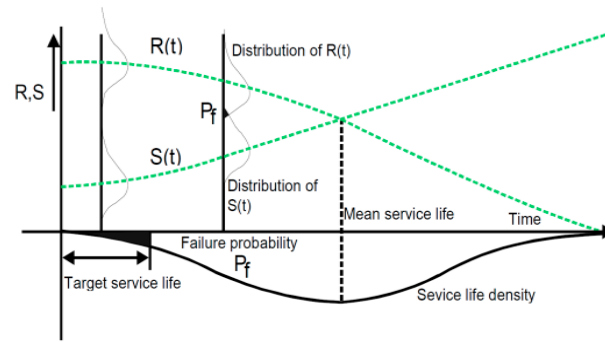


Figure 11. Events during a service life.



**Figure 12.** Probability of failure and target service life.

$$P_f(T) = 1 - P\{g(x, t) > 0, t \in [0, T]\} \quad (5)$$

$$g(x, t) = R(t) - S(t) \quad (6)$$

$$\frac{C_{cr}}{\gamma_{C_{cr}}} - A_{C_{s,cl}} \cdot \left(\frac{w}{b}\right) \cdot \gamma_{C_{s,cl}} \left[ 1 - \operatorname{erf} \left( \frac{x - \Delta x}{2 \sqrt{\gamma_{R_{cl}} \cdot k_{e,cl} \cdot k_{c,cl} D_{RCM,0} \left(\frac{t_0}{t}\right)^{n_{cl}} \cdot t}} \right) \right] = 0 \quad (7)$$

where  $R(t)$  and  $S(t)$  are the time-variant resistance and the load variable, respectively;  $C_{cr}$  is the eigenvalue of the critical chloride ion concentration;  $\gamma_{C_{cr}}$  is the fractional coefficient of the critical chloride ion concentration;  $A_{C_{s,cl}}$  is the regression coefficient of the chloride ion concentration at the concrete surface and the water/cement ratio relationship in concrete;  $w/b$  is the water/cement ratio;  $\gamma_{C_{s,cl}}$  is the fractional coefficient of the chloride concentration at the concrete surface;  $X$  is the cover thickness (mm);  $\Delta x$  is the construction deviation of the cover thickness (mm);  $\gamma_{R_{cl}}$  is the fractional coefficient of chloride ion diffusion;  $k_{e,cl}$  is the environment influencing the coefficient of chloride ion diffusion;  $k_{c,cl}$  is the curing coefficient of chloride ion diffusion;  $D_{RCM,0}$  is the coefficient of chloride ion diffusion;  $t_0$  is the testing time during the diffusion test;  $n_{cl}$  is the degradation coefficient of chloride diffusion;  $t$  is the design life span of the structure. Further, the error formula is  $\operatorname{erf}(x) = \frac{2}{\sqrt{\pi}} \int_0^x e^{-y^2} dy$ .

As mentioned above, both the load level and temperature affect the chloride diffusion coefficient of concrete. The loading factor ' $k_s$ ' and temperature factor ' $k_t$ ' were introduced into the model, and they are shown, respectively, in Equations (8) and (9). It is worth noting that the revised DuraCrete model (Equation (8)) was improved from Equation (7), whose chloride diffusion coefficient  $D_{RCM,0}$  was multiplied by the loading factor ' $k_s$ ' and temperature factor ' $k_t$ ' in order to enlarge the chloride diffusion coefficient considering the effect of the two parameters. Reference [35] highlighted the temperature factor, which needs to be further considered, and in Equation (9),  $T$  is the monthly average temperature monitored by embedded relative temperature and humidity sensors. According to Equation (9), it was concluded that different monthly values contribute to various mean values of temperature factor ' $k_t$ '. As shown in Figure 10, the minimum value of average monthly temperature was 2 °C (275 K) and the maximum was 28 °C (301 K), respectively. Correspondingly, the minimum and maximum values of ' $k_t$ ' were 0.41 and 1.31, respectively. Even if the maximum ' $k_t$ ' value were to be used, resulting in the minimum value of the remaining service life, it would still satisfy the designed service life of 100 years.

$$\frac{C_{cr}}{\gamma_{C_{cr}}} - A_{C_{s,cl}} \cdot \left(\frac{w}{b}\right) \cdot \gamma_{C_{s,cl}} \left[ 1 - \operatorname{erf} \left( \frac{x - \Delta x}{2 \sqrt{\gamma_{R_{cl}} \cdot k_{e,cl} \cdot k_{c,cl} \cdot k_s \cdot k_t \cdot D_{RCM,0} \left(\frac{t_0}{t}\right)^{n_{cl}} \cdot t}} \right) \right] = 0 \quad (8)$$

where  $k_s$  is the loading factor,  $k_t$  is the temperature factor,  $q$  is the constant of the average

$$k_t = \frac{T}{T_0} \exp \left[ q \left( \frac{1}{T_0} - \frac{1}{T} \right) \right] \quad (9)$$

activation energy ( $q = 3739$  K for PFA and  $q = 2776$  K for OPC [35]), and  $T_0 = 293$  K (20 °C).

Using Equation (10), the surface chloride ion concentration of the concrete can be calculated. The characteristic values of the regression parameter  $A_{C_{s,cl}}$  and critical chloride concentration  $C_{CR}$  for different types of concrete in different corrosion zones are shown in Tables 4 and 5, respectively.

$$C_{s,cl} = A_{C_{s,cl}} \cdot \left(\frac{w}{b}\right) \gamma_{C_{s,cl}} \quad (10)$$

**Table 4.** Characteristic values of the regression parameter  $A_{C_{s,cl}}$  (% relative to binder).

	OPC	PFA	GGBS	SF
<b>Atmospheric</b>	2.57	4.42	3.05	3.23
<b>Tidal and Splash</b>	7.76	7.45	6.77	7.96
<b>Submerged</b>	10.3	10.8	5.06	12.5

**Table 5.** Characteristic values of the critical chloride concentration  $C_{cr}$  (% relative to binder).

	Water/cement ratio (w/b) = 0.3	w/b = 0.4	w/b = 0.5
<b>Submerged</b>	2.3	2.1	1.6
<b>Splash and Tidal</b>	0.9	0.8	0.5

The chloride ion diffusion coefficient of concrete decreases with exposure time, and is inversely proportional to corrosion time [36–39]. Further, the age factors of different types of concrete in different corrosion zones are shown in Table 6. It is worth mentioning that the chloride ion diffusion coefficient  $D_{RCM,0}$  decreases with time, and actually stabilizes gradually as time increases, to a certain degree. In this model,  $D_{RCM,0}$  is modified through the change in the age factor  $n_{cl}$ , and  $D_{RCM,0}$  is obtained through a short-time RCM test. Hence, the age factor  $n_{cl}$  corresponds to the instantaneous chloride diffusion coefficient in this paper.

**Table 6.** Age factor of the chloride diffusion coefficient  $n_{cl}$ .

	OPC	PFA	GGBS	SF
<b>Atmospheric</b>	0.65	0.66	0.85	0.79
<b>Tidal and Splash Zones</b>	0.37	0.93	0.60	0.39
<b>Submerged</b>	0.30	0.69	0.71	0.62

Additionally, chloride ions' penetration into concrete is affected by the environment and the curing age [40]. The chloride diffusion coefficient can be expressed by Equations (11) and (12), and the characteristic values of the environment factor and the curing factor are shown in Tables 7 and 8. Further, the partial factors relevant for structures in a marine environment are shown in Table 9.

**Table 7.** Characteristic values of the environment factor  $k_{e,cl}$ .

	OPC	GGBS
<b>Atmospheric</b>	0.68	1.98
<b>Splash Zone</b>	0.27	0.78
<b>Tidal Zone</b>	0.92	2.70
<b>Submerged</b>	1.32	3.88

**Table 8.** Characteristic values of the curing factor  $k_{c,cl}$ .

Curing Time	1 d	3 d	7 d	28 d
$k_{c,cl}$	2.08	1.50	1	0.79

**Table 9.** Partial factors for structures in a marine environment.

Cost of Mitigation of Risk Relative to the Cost of Repair	High	Normal	Low
$\Delta x$ (mm)	20	14	8
$\gamma_{C_{cr}}$	1.20	1.06	1.03
$\gamma_{C_{s,cl}}$	1.70	1.40	1.20
$\gamma_{R_{cl}}$	3.25	2.35	1.50

$$D_t = \gamma_{R_{cl}} \cdot k_{e,cl} \cdot k_{c,cl} \cdot k_s \cdot k_t \cdot D_{RCM,0} \left( \frac{t_0}{t} \right)^{n_{cl}} \cdot t \quad (11)$$

$$D_{RCM,0} \text{ (mm}^2/\text{year)} = D_{RCM,28\text{days}} \text{ (m}^2/\text{s)} \times 3.1536 \times 10^{13} \quad (12)$$

According to Equation (8), the chloride diffusion coefficient  $D_{RCM}$  and the cover thickness  $x$  are the most significant factors that affect the service life of a concrete structure. In order to investigate the target reliability  $\beta$ , Monte-Carlo (MC) simulations were carried out using the software Matlab in order to provide further evidence for the durability performance assessment (Figure 13). The acceptance criterion was defined in terms of the reliability index,  $\beta$ , as follows:

$$\beta = -\Phi^{-1}(P_f) \quad (13)$$

where  $P_f$  is the probability of the considered event occurring within the considered reference period (service life).

According to the Chinese unified standard for reliability design of building structures (GB 50068-2017), the calculation formula of the reliability index  $\beta$  is shown as Equation (13). The reliability index  $\beta$  is relevant to the failure probability  $P_f$ , and the relationship between the two factors is shown in Table 10. In this paper,  $\beta = 1.645$  (5% failure probability) was regarded as a target reliability because the construction is not allowed to be repaired during the designed service life. Based on the results of the reliability analyses carried out by the partial factor method, the risk acceptance criterion was defined.

```

l=0:0.1:100 → Designed service life
mu1=52 → Mean value of cover thickness
sigal=5.21 → Standard deviation of X
D=normrnd(73.2,3.14,100,1) → Mean and standard deviation of  $D_{RCM}$ 
s=2.*erfinv(1-0.9/3.80).*sqrt(D*1) (mm2/year)
[mu2,siga2]=normfit(s) → Surface chloride concentration
mu=mu1-mu2 Critical chloride concentration
siga=sqrt(sigal.*sigal+siga2.*siga2)
p=mu./siga
plot(l,p)
grid

```

**Figure 13.** Programming language of Monte-Carlo simulation.



**Table 10.** Relationship between the failure probability  $P_f$  and the reliability index  $\beta$ .

Failure Probability $P_f$	Reliability Index $\beta$
5%	1.645
10%	1.282

## 5. Service Life Predictions

### 5.1. Reinforced Concrete in the Marine Section

Chloride penetration into concrete is much more severe than carbonation-induced corrosion of reinforced bars in concrete structures in marine environments. Therefore, only chloride-induced corrosion of reinforced bars was considered, and the revised DuraCrete model (Equation (8)) was used to predict the service life of a concrete structure. Since it is difficult to measure the concrete cover thicknesses of the box girder and platform, the designed cover thicknesses and the corresponding standard deviations with assumptions were used in the service life prediction calculations. On the other hand, the measured concrete cover thickness of the pier concrete was used in the service life prediction calculations. Figure 14 shows a photograph of the Jiaozhou Bay sea-crossing railway bridge in its completed state.

**Figure 14.** Jiaozhou Bay sea-crossing railway bridge (completed).

#### 5.1.1. Box Girder Concrete

The box girder concrete located in the atmospheric zones and carbon reinforced bars were used in this structure. The characteristic value of the critical chloride concentration  $C_{cr}$  is 0.9% relative to the binder. The characteristic value of the regression parameter  $A_{C_{s,cl}}$  is 4.42%, and that of the age factor  $n_{cl}$  is 0.66 because w.t. 30% fly ash replacement of cement was used in the concrete. The characteristic value of the concrete cover  $x$  is 50 mm (designed value), and the margin for the concrete cover  $\Delta x$  is 8 mm. The main durability parameters used in the service life prediction model are shown in Table 11. After curing for 28 days, the measured apparent chloride diffusion coefficient of the box girder concrete is  $2.32 \times 10^{-12} \text{ m}^2/\text{s}$ . The reliability indexes of the box girder concrete for different service lives were calculated and are shown in Figure 15, and then  $t = 223.9$  years and reliability index  $\beta = 1.81$  were calculated for when the box girder concrete service life is 100 years.

**Table 11.** Parameters used in the revised DuraCrete model in the marine section.

Parameters	$\gamma_{C_{cr}}$ (-)	$C_{cr}$ (%)	$A_{C_{s,cl}}$ (%)	$\gamma_{C_{s,cl}}$ (-)	$X$ (mm)	$\Delta x$ (mm)	$\gamma_{R_{cl}}$ (-)	$k_{e,cl}$ (-)	$k_{c,cl}$ (-)	$n_{cl}$ (-)	$w/b$ (-)
Box girder	1.2	0.9	4.42	1.7	50	8	3.25	0.68	0.79	0.66	0.3
Pier	1.2	0.9/4.5	7.46	1.7	52	5.21	3.25	0.27	0.79	0.93	0.3
Platform	1.03	2.3	10.8	1.2	60	8	1.5	1.32	0.79	0.69	0.3

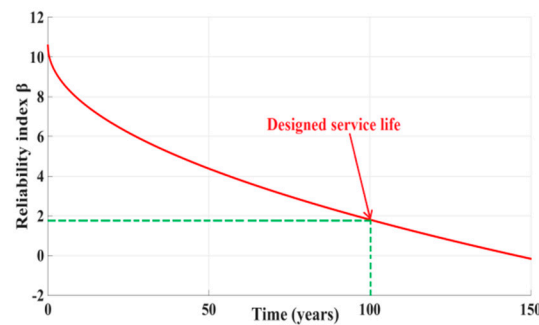


**Figure 15.** Reliability index calculated by the Monte-Carlo simulation for the box girder concrete.

### 5.1.2. Pier Concrete

Corrosion-resistant reinforced bars were used to improve the durability of the reinforced concrete. The characteristic value of the concrete cover  $x$  is 52 mm, and the margin for the concrete cover  $\Delta x$  is 5.21 mm. After curing for 28 days, the measured apparent chloride diffusion coefficient of the pier concrete was  $2.32 \times 10^{-12} \text{ m}^2/\text{s}$ . The main durability parameters used in the service life prediction model are shown in Table 11. The reliability indexes of the pier concrete with carbon reinforced bars and with corrosion-resistant reinforced bars were calculated and are shown in Figure 16.

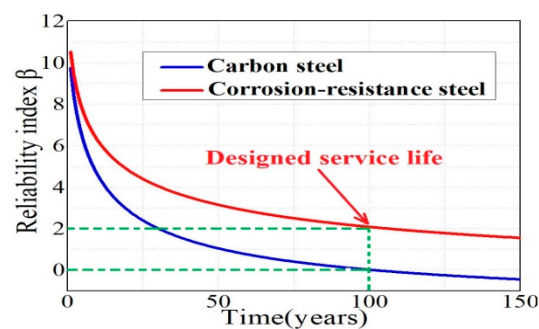


**Figure 16.** Reliability index calculated by the Monte-Carlo simulation for the pier concrete.

Table 11 shows that the critical chloride concentration for the carbon reinforced bars in the splash zone is 0.9%. On the other hand, as the corrosion-resistant reinforced bars are more corrosion-resistant, the critical chloride concentration for the corrosion-resistant reinforced bars in the splash zone is 4.5% [41–43]. For the pier concrete with carbon reinforced bars, the reliability index of the reinforced concrete after 100 years of service is only 0.03. On the other hand, for the pier concrete with corrosion-resistant reinforced bars, the reliability index of the reinforced concrete after 100 years of service is nearly 2.0. The higher reliability index can be attributed to the higher critical chloride concentration in the corrosion-resistant reinforced bars as compared to that in the carbon reinforced bars. Further, the service life of the pier with corrosion-resistant reinforced bars in the marine section is 263.2 years, and its reliability index is 2.01 when serving for 100 years.

### 5.1.3. Platform Concrete

For the platform concrete located in the submerged zone, the designed characteristic value of the concrete cover  $x$  is 60 mm, and the margin for the concrete cover  $\Delta x$  is 8 mm. Since it is difficult to repair the platform concrete, the partial factor for the critical chloride concentration  $\gamma_{C_{cr}}$  is 1.03. The main durability parameters used in the service life prediction model are shown in Table 11. The reliability indexes of the platform concrete for different service years were calculated and are shown in Figure 17. The service life is 113.6 years and the reliability index is 1.76 for the platform concrete with 100 service years.

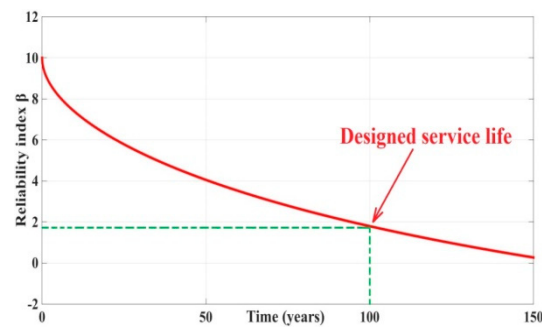


**Figure 17.** Reliability index calculated by the Monte-Carlo simulation for the platform concrete.

### 5.2. Reinforced Concrete in the Land Section

The reinforced concrete in the Jiaozhou Bay sea-crossing railway bridge in the land section was mainly damaged by salt fog, and concrete with a compressive strength grade of C40 and a cover thickness of 35 mm was used. The service environment of the reinforced concrete in the land section can be divided into atmospheric zones, and the mainly durability parameters are listed in Table 12. The apparent chloride diffusion coefficient was  $4.38 \times 10^{-12} \text{ m}^2/\text{s}$ , and the concrete cover thickness was 36 mm with a margin of 3.18 mm. The reliability index of the reinforced concrete located in the land section, in service for 100 years, is 1.71, while the predicted service life is 173.8 years, which meets the designed service life requirement (Figure 18).

**Table 12.** Parameters used in the revised DuraCrete model in the land section.

Parameters	$\gamma_{C_{cr}}$ (-)	$C_{cr}$ (%)	$A_{C_{s,cl}}$ (%)	$\gamma_{C_{s,cl}}$ (-)	$X$ (mm)	$\Delta x$ (mm)	$\gamma_{R_{cl}}$ (-)	$k_{e,cl}$ (-)	$k_{c,cl}$ (-)	$n_{cl}$ (-)	$w/b$ (-)
Land Section	1.2	2.24	7.46	1.7	36	3.18	3.25	0.92	0.79	0.93	0.33

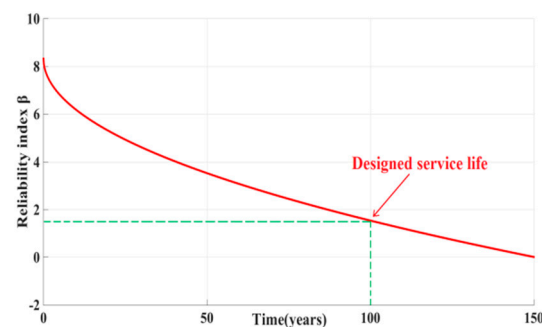


**Figure 18.** Reliability index calculated by the Monte-Carlo simulation (land section).

## 6. Conclusions

This paper discusses the influence of cover thickness, compressive strength, chloride diffusion coefficient, and surface defects, as well as the micro-environment of concrete on the service life of the Jiaozhou Bay sea-crossing railway bridge. The temperature and relative humidity in the concrete and the loading applied onto the reinforced concrete were measured. For the reinforced concrete in the service environment of the bridge, the service life prediction model was revised according to suggestions by DuraCrete. The main durability parameters were determined based on DuraCrete guidelines and the measured results. Further, using the revised model, the reliability indexes of the service life of concrete with carbon reinforced bars and with corrosion-resistant reinforced bars were calculated. Based on the measured data and the analyses, as described in this paper, the conclusions are as follows:

1. According to the in situ measurements, the actual mean compressive strength of the concrete is higher than the designed value, while the maximum difference between the measured and designed cover thicknesses of the concrete piers is less than 15 mm. Due to the non-uniform vibration during concreting, there are defects on the concrete surface. Further, the temperature at the concrete surface varies with the atmospheric temperature. The applied load testing shows that the concrete structure suffers the effect of loading, which results in a larger chloride diffusion coefficient.

2. According to the suggestions by DuraCrete, the model was revised by adding two parameters, i.e., the loading factor ' $k_s$ ' and the temperature factor ' $k_t$ '. The added parameters affect the service life prediction; moreover, the revised prediction model was used in the service life predictions.

3. The partial factor method and Monte-Carlo simulations were used to predict the service life and the reliability index. The results show that by comparing the concrete in the marine and land sections, the predicted remaining service life of the Jiaozhou Bay sea-crossing railway bridge can meet the designed 100 years, based on the revised DuraCrete model. Additionally, the reliability index calculations based on the Monte-Carlo simulations show that the results of the partial factor method are relatively reliable.

**Author Contributions:** Conceptualization, Z.J. and T.Z.; Formal analysis, Z.L.; Investigation, Z.L.; Methodology, Z.J. and T.Z.; Resources, Z.J. and T.Z.; Software, P.W.; Supervision, Z.J. and T.Z.; Writing-original draft, Z.L.; Writing-review and editing, Z.L., C.X., Y.K. and L.Z.; For other cases, all authors have contributed equally.

**Funding:** National Key R&D Program of China Grant No. 2017YFB0310000, Key Research and Development Program of Shandong Province No. 2019GGX102053, National Natural Science Foundation of China (NSF) Grant No. 51678318, 51709253, 51420105015 and 51608286, Chinese National 973 projects Grant No. 2015CB655100, 111 Project and Chinese Scholarship Council (CSC).

**Conflicts of Interest:** The authors declare no conflict of interest.

## References

1. Mou, B.; Li, X.; Qiao, Q.Y.; He, B.J.; Wu, M.L. Seismic behavior of frame corner joints under bidirectional cyclic loading test. *Eng. Struct.* **2019**, *196*, 109316. [[CrossRef](#)]
2. Mou, B.; Bai, Y.T. Experimental investigation on shear behavior of H-shaped beam-to-CFST column connections with irregular panel zone. *Eng. Struct.* **2018**, *168*, 487–504. [[CrossRef](#)]
3. Qiao, Q.Y.; Zhang, W.W.; Mou, B.; Cao, W.L. Seismic behavior of exposed concrete filled steel tube column bases with embedded reinforcing bars: Experimental investigation. *Thin Walled Struct.* **2019**, *136*, 367–381. [[CrossRef](#)]
4. Rostam, S.; Faber, M. Probabilistic Performance Based Durability Design of Concrete Structures. In *Nordic Concrete Research*; Norsk Betongforening: Espoo, Finland, 1996.
5. Chang, H.L. Chloride binding capacity of pastes influenced by carbonation under three conditions. *Cem. Concr. Compos.* **2017**, *84*, 1–9. [[CrossRef](#)]
6. Chang, H.L.; Mu, S.; Feng, P. Influence of carbonation on “maximum phenomenon” under cyclic wetting and drying condition. *Cem. Concr. Res.* **2018**, *103*, 95–109. [[CrossRef](#)]
7. Li, N.; Farzadnia, N.; Shi, C. Microstructural changes in alkali-activated slag mortars induced by accelerated carbonation. *Cem. Concr. Res.* **2017**, *100*, 214–226. [[CrossRef](#)]
8. Yu, Y.; Zhu, H. Influence of Rubber Size on Properties of Crumb Rubber Mortars. *Materials* **2016**, *9*, 527. [[CrossRef](#)] [[PubMed](#)]
9. Chang, H.; Mu, S.; Xie, D.; Wang, P. Influence of pore structure and moisture distribution on chloride “maximum phenomenon” in surface layer of specimens exposed to cyclic drying-wetting condition. *Constr. Build. Mater.* **2017**, *131*, 16–30. [[CrossRef](#)]
10. Li, Z.; Jin, Z.; Zhao, T.; Wang, P.; Li, Z.; Xiong, C.; Zhang, K. Use of a novel electro-magnetic apparatus to monitor corrosion of reinforced bar in concrete. *Sens. Actuators A Phys.* **2019**, *286*, 14–27. [[CrossRef](#)]
11. Xiong, C.; Li, W.; Jin, Z.; Gao, X.; Wang, W.; Tian, H.; Han, P.; Song, L.; Jiang, L. Preparation of phytic acid conversion coating and corrosion protection performances for steel in chlorinated simulated concrete pore solution. *Corros. Sci.* **2018**, *139*, 275–288. [[CrossRef](#)]



12. Xiong, C.; Jiang, L.; Xu, Y.; Chu, H.; Jin, M.; Zhang, Y. Deterioration of pastes exposed to leaching, external sulfate attack and the dual actions. *Constr. Build. Mater.* **2016**, *116*, 52–62. [[CrossRef](#)]
13. Zhu, W.J.; Francois, R.; Zhang, C.P.; Zhang, D.L. Propagation of corrosion-induced cracks of the RC beam exposed to marine environment under sustained load for a period of 26 years. *Cem. Concr. Res.* **2018**, *103*, 66–76. [[CrossRef](#)]
14. Zhang, X.; Wang, J.; Zhao, Y.; Tang, L.; Xing, F. Time-dependent probability assessment for chloride induced corrosion of RC structures using the third-moment method. *Constr. Build. Mater.* **2015**, *76*, 232–244. [[CrossRef](#)]
15. Wu, L.; Li, W.; Yu, X. Time-dependent chloride penetration in concrete in marine environments. *Constr. Build. Mater.* **2017**, *152*, 406–413. [[CrossRef](#)]
16. Wang, Y.; Wu, L.; Wang, Y.; Li, Q.; Xiao, Z. Prediction model of long-term chloride diffusion into plain concrete considering the effect of the heterogeneity of materials exposed to marine tidal zone. *Constr. Build. Mater.* **2018**, *159*, 297–315. [[CrossRef](#)]
17. Attari, A.; McNally, C.; Richardson, M.G. A probabilistic assessment of the influence of age factor on the service life of concretes with limestone cement/GGBS binders. *Constr. Build. Mater.* **2016**, *111*, 488–494. [[CrossRef](#)]
18. Yu, H.F.; Ma, H.X.; Yan, K. An equation for determining freeze-thaw fatigue damage in concrete and a model for predicting the service life. *Constr. Build. Mater.* **2017**, *137*, 104–116. [[CrossRef](#)]
19. Yu, H.; Da, B.; Ma, H.; Zhu, H.; Yu, Q.; Ye, H.; Jing, X. Durability of concrete structures in tropical atoll environment. *Ocean Eng.* **2017**, *135*, 1–10. [[CrossRef](#)]
20. Hackl, J.; Kohler, J. Reliability assessment of deteriorating reinforced concrete structures by representing the coupled effect of corrosion initiation and progression by Bayesian networks. *Struct. Saf.* **2016**, *62*, 12–23. [[CrossRef](#)]
21. Yu, H.F.; Sun, W.; Yan, L.H.; Ma, H.Y. Study on prediction of concrete service life I-theoretical model. *J. Chin. Ceram. Soc.* **2002**, *30*, 686–690. (In Chinese)
22. Poupard, O.; L'Hostis, V.; Catinaud, S.; Petre-Lazar, I. Corrosion damage diagnosis of a reinforced concrete beam after 40 years natural exposure in marine environment. *Cem. Concr. Res.* **2006**, *36*, 504–520. [[CrossRef](#)]
23. Marchand, J.; Samson, E. Predicting the service-life of concrete structures—Limitations of simplified models. *Cem. Concr. Compos.* **2009**, *31*, 515–521. [[CrossRef](#)]
24. Jin, Z.Q.; Zhao, T.J.; Hou, B.R.; Li, Q.Y. Service life prediction of lining concrete for Jiaozhou Bay Subsea Tunnel. *J. Civ. Archit. Environ. Eng.* **2009**, *31*, 86–91. (In Chinese)
25. Jin, Z.Q.; Sun, W.; Hou, B.R.; Zhang, P. Key parameters of constructed lining concrete in Jiaozhou Bay Subsea Tunnel. *J. Cent. South Univ. Sci. Technol.* **2011**, *42*, 810–816. (In Chinese)
26. Ai, Z.Y.; Jiang, J.Y.; Sun, W.; Song, D.; Ma, H.; Zhang, J.C.; Wang, D.Q. Passive behavior of alloy corrosion-resistant steel Cr10Mo1 in simulating concrete pore solutions with different pH. *Appl. Surf. Sci.* **2016**, *389*, 1126–1136. [[CrossRef](#)]
27. Ai, Z.Y.; Sun, W.; Jiang, J.Y.; Song, D.; Ma, H.; Zhang, J.C.; Wang, D.Q. Corrosion-resistant steel Cr10Mo1 in simulating concrete pore solutions: Combination effects of pH and chloride. *Materials* **2016**, *9*, 749. [[CrossRef](#)]
28. Tang, L.P. Engineering expression of the ClinConc model for prediction of free and total chloride ingress in submerged marine concrete. *Cem. Concr. Res.* **2008**, *38*, 1092–1097.
29. Zhao, T.J.; Jin, Z.Q.; Wang, M.P.; Zhao, J.Z. Environmental condition and durability of lining concrete in Jiaozhou Bay Subsea Tunnel. *Chin. J. Rock Mech. Eng.* **2007**, *26*, 3823–3829. (In Chinese)
30. Jin, Z.; Zhao, X.; Zhao, T.; Yang, L. Interaction between compressive load and corrosive-ion attack on reinforced concrete with accelerated potentiostatic corrosion. *Constr. Build. Mater.* **2016**, *113*, 805–814. [[CrossRef](#)]
31. Xu, J.; Li, F.; Zhao, J.; Huang, L. Model of time-dependent and stress-dependent chloride penetration of concrete under sustained axial pressure in the marine environment. *Constr. Build. Mater.* **2018**, *170*, 207–216. [[CrossRef](#)]
32. Wan, X.M.; Su, Q.; Zhao, T.J.; Ren, X.B. Micro-cracking and chloride penetration of concrete under uniaxial compression. *J. Civ. Archit. Environ. Eng.* **2013**, *35*, 104–110. (In Chinese)
33. Zhao, R.; Jin, Z.Q.; Cao, J.R.; Du, F.Y.; Kang, Y. Numerical simulation of chloride ions transportation considering temperature and humidity in marine environment. *Ocean Eng.* **2018**, *36*, 99–106. (In Chinese) [[CrossRef](#)]

34. Zhao, L.X.; Wang, P.G.; Zhao, T.J.; Wang, L.Q.; Tian, Y.P.; Wang, Y. Research on temperature action spectrum and temperature response of concrete under natural environment in Qingdao. *Bull. Chin. Ceram. Soc.* **2018**, *37*, 2770–2774. (In Chinese)
35. Amey, S.L.; Johnson, D.A.; Miltenberger, M.A. Predicting the service life of concrete marine structures: An environmental methodology. *ACI Struct. J.* **1998**, *95*, 205–214.
36. Bao, J.W.; Wang, L.C. Combined effect of water and sustained compressive loading on chloride penetration into concrete. *Constr. Build. Mater.* **2017**, *156*, 708–718. [[CrossRef](#)]
37. Wang, L.; Bao, J.; Ueda, T. Prediction of mass transport in cracked-unsaturated concrete by mesoscale lattice model. *Ocean Eng.* **2016**, *127*, 144–157. [[CrossRef](#)]
38. Bao, J.W.; Wang, L.C. Effect of short-term sustained uniaxial loadings on water absorption of concrete. *J. Mater. Civ. Eng.* **2017**, *29*, 04016234. [[CrossRef](#)]
39. Petcherdchoo, A. Time dependent models of apparent diffusion coefficient and surface chloride for chloride transport in fly ash concrete. *Constr. Build. Mater.* **2013**, *38*, 497–507. [[CrossRef](#)]
40. Yu, Z.; Ye, G. New perspective of service life prediction of fly ash concrete. *Constr. Build. Mater.* **2013**, *48*, 764–771. [[CrossRef](#)]
41. Li, K.F.; Li, Q.W.; Zhou, X.G.; Fan, Z.H. Durability design of the Hong Kong-Zhuhai-Macao Sea-Link Project: Principle and procedure. *J. Bridge Eng.* **2015**, *20*, 341–352. [[CrossRef](#)]
42. Li, Q.W.; Li, K.F.; Zhou, X.G.; Zhang, Q.M.; Fan, Z.H. Model-based durability design of concrete structures in Hong Kong-Zhuhai-Macao Sea-Link Project. *Struct. Saf.* **2015**, *53*, 1–12. [[CrossRef](#)]
43. Ai, Z.Y.; Sun, W.; Jiang, J.Y.; Ma, H.; Zhang, J.C.; Song, D. Passive behavior of new alloy corrosion resistant steel Cr<sub>10</sub>Mo<sub>1</sub> in chloride-containing environment. *Mater. Rev.* **2016**, *30*, 92–118. (In Chinese)



© 2019 by the authors. Licensee MDPI, Basel, Switzerland. This article is an open access article distributed under the terms and conditions of the Creative Commons Attribution (CC BY) license (<http://creativecommons.org/licenses/by/4.0/>).